International Journal of Thermal Sciences 115 (2017) 197–209

Contents lists available at ScienceDirect

International Journal of Thermal Sciences

journal homepage: www.elsevier.com/locate/ijts

Condensation heat transfer of R245fa in a shell-tube heat exchanger at slightly inclined angles

Shuang Cao [a], Jinliang Xu [a, *], Yuzhang Li [a], Yuying Yan [b, **]

[a] The Beijing Key Laboratory of Multiphase Flow and Heat Transfer, North China Electric Power University, Beijing, 102206, China
[b] Energy & Sustainability Research Division, Faculty of Engineering, University of Nottingham, University Park, Nottingham NG7 2RD, UK

ARTICLE INFO

Article history:
Received 26 September 2016
Received in revised form
6 January 2017
Accepted 31 January 2017

Keywords:
Condensation
Heat transfer
Flow pattern
Organic Rankine cycle

ABSTRACT

Condensation heat transfer of R245fa was investigated in a shell-tube condenser. The copper tube had an inner diameter of 14.70 mm with a 1600 mm heat transfer length. Mass fluxes and vapor mass qualities covered ranges of 198.8–504.7 kg/m^{2}s and 0.291–0.976, respectively. Condensation heat transfer coefficients are increased with increases of mass fluxes and vapor mass qualities. The horizontal position yielded minimum condensation heat transfer coefficients. Deviating from the horizontal position enhances condensation heat transfer. The condenser is suggested to operate at weakly inclined flow to reach better thermal performance. Flow patterns and liquid height signals explored the condensation heat transfer mechanisms. The flow is stable for inclined down-flow but becomes unstable for inclined up-flow, which was caused by the vapor-liquid interface wave. Non-dimensional parameter analysis identified the competition between inertia force and gravity force. The vapor-liquid interface wave is the mechanism to enhance condensation heat transfer for inclined up-flow, while the decreased liquid film thickness on the tube bottom enhances heat transfer enhancement for inclined down-flow. A correlation based on the Froude number of vapor phase successfully matched the experimental data. This study is useful for the condenser design and operation such as applied in Organic Rankine Cycles.

1. Introduction

Many engineering applications need better understanding of phase change heat transfer of organic fluids in tubes or heat exchangers. Topics include evaporation or condensation heat transfer coefficients, pressure drops, critical heat fluxes, flow instabilities etc, which significantly influence fabrication cost, operation, and efficiency of energy conversion systems. Air-conditioning or refrigeration industries widely use organic fluids to complete the refrigeration cycle [1–4]. Most refrigeration facilities have power capacities in the range of 1–10 kW [5,6], at which small diameter tube such as 8.0 mm is widely used. Another progressing application is the organic Rankine cycle (ORC) for low grade energy utilization [7,8]. ORCs are useful to increase energy utilization efficiency and reduce carbon dioxide (CO_2) emission. Compared with refrigeration application, large scale utilization of ORCs needs larger diameter tubes for heat transfer and conversion.

Both engineering areas are looking for better organic fluids. Organic fluids shall have good physical/chemical properties to have high heat transfer coefficients, low pressure drops and low environment impact, comprehensively. R245fa (1, 1, 1, 3, 3-pentafluoropropane, $CF_3CH_2CHF_2$, molecular weight of 134) is a preferred fluid, having zero Ozone Depletion Index (ODI) and lower Greenhouse Effect Index [9]. Thus, it has potential to expand its application in various industries [10–12]. R245fa has a saturation temperature of 15.14 °C, 9% latent heat and 25% surface tension force of water, at atmospheric pressure.

Studies on R245fa phase change hat transfer are not enough to support industry applications, especially in larger tubes or heat exchangers [13]. Some R245fa condensation heat transfer studies are reported in capillary tubes below or around 8.0 mm for refrigeration applications. Cavallini et al. [14] investigated condensation heat transfer in a 0.96 mm capillary tube at 40°C saturation temperature with fluids of R32 and R245fa. They found that, even though R32 has higher liquid thermal conductivity than R245fa by 34%, the two fluids almost have identical condensation heat transfer coefficients with similar mass fluxes and vapor mass

* Corresponding author.
** Corresponding author.
E-mail addresses: xjl@ncepu.edu.cn (J. Xu), Yuying.Yan@nottingham.ac.uk (Y. Yan).

http://dx.doi.org/10.1016/j.ijthermalsci.2017.01.029
1290-0729/

qualities, due to increased shear stress on the tube wall induced by higher vapor velocity for R245fa. Al-Hajri et al. [15] experimentally characterized condensing flows of R134a and R245fa in a single microchannel with a cross-section of 0.4 mm by 2.8 mm (aspect ratio of 7:1) and a length of 190 mm. They showed that the saturation temperature and mass flux have significant effects on both heat transfer coefficients and pressure drops, but the inlet superheating degree has little or no effect. Ghim and Lee [16] showed that even though *n*-pentane has larger liquid thermal conductivity and latent heat of evaporation than R245fa, its easy combustion characteristic limits the application in ORCs.

In fact, phase change heat transfer is related to flow patterns in tubes. Lips & Meyer [17] measured condensation flow patterns and heat transfer of R134a in a 8.38 mm inner diameter tube. The flow direction is from vertical down-flow to up-flow. Stratified-wavy flow was dominant at low mass fluxes and vapor mass qualities, under which heat transfer was sensitive to inclination angles. Heat transfer was insensitive to inclination angles in annular flow regime at high mass fluxes and vapor mass qualities. Condensation heat transfer coefficients reached maximum for downward flow at $\theta = -15°$~$-30°$ and minimum for upward flow at $\theta = 15°$. Mohseni et al. [18] investigated flow patterns and heat transfer of R134a in a tube with 8.38 mm in diameter, they found that condensation heat transfer coefficients reached maximum at $\theta = 30°$ (up-flow) for low vapor mass qualities but reached maximum at the horizontal position with high vapor mass qualities. Thus, conclusions by Mohseni et al. [18] and Lips & Meyer [17] are different. Gupta et al. [19] gave non-dimensional parameters in two-phase systems, such as Reynolds number (inertia force relative to viscous force), Froude number (inertia force relative to gravity), Bond number (gravity force relative to surface tension), capillary number (viscous force relative to surface tension), and Weber number (inertia force relative to surface tension). Gravity force is involved in Froude and Bond numbers. The tube diameter is involved in all the dimensionless parameters except capillary number. Flow patterns are strongly dependent on inclination angles, so as to affect condensation heat transfer.

In summary, few studies are reported on R245fa condensation heat transfer in larger diameter tubes or heat exchangers. This paper investigated condensation heat transfer in a shell-tube condenser (heat exchanger). The cooling capacity is up to 15 kW, which may be the maximum limit in laboratory scale. The whole heat exchanger was running at inclination angles from $-30°$ (inclined down-flow) to $30°$ (inclined up-flow). We found that condensation heat transfer coefficients reached minimum values at the purely horizontal position. Both inclined up-flow and down-flow enhance condensation heat transfer. In order to understand the mechanisms, we performed flow visualization studies. The inertia force, gravity force and interface wave are competed with each to obtain the peculiar condensation heat transfer distributions regarding the inclination angle effect. For inclined up-flow, the interface wave is the mechanism for heat transfer enhancement. Alternatively, the inclined down-flow weakens the liquid film thickness at the tube bottom to account for the heat transfer enhancement. Our findings suggest the slightly inclined condenser position to improve the thermal performance of R245fa condensers.

2. The experimental details

2.1. Experimental setup

Fig. 1 shows the experimental setup, consisting of a forced convective R245fa fluid loop, a regenerative heat exchanger, a

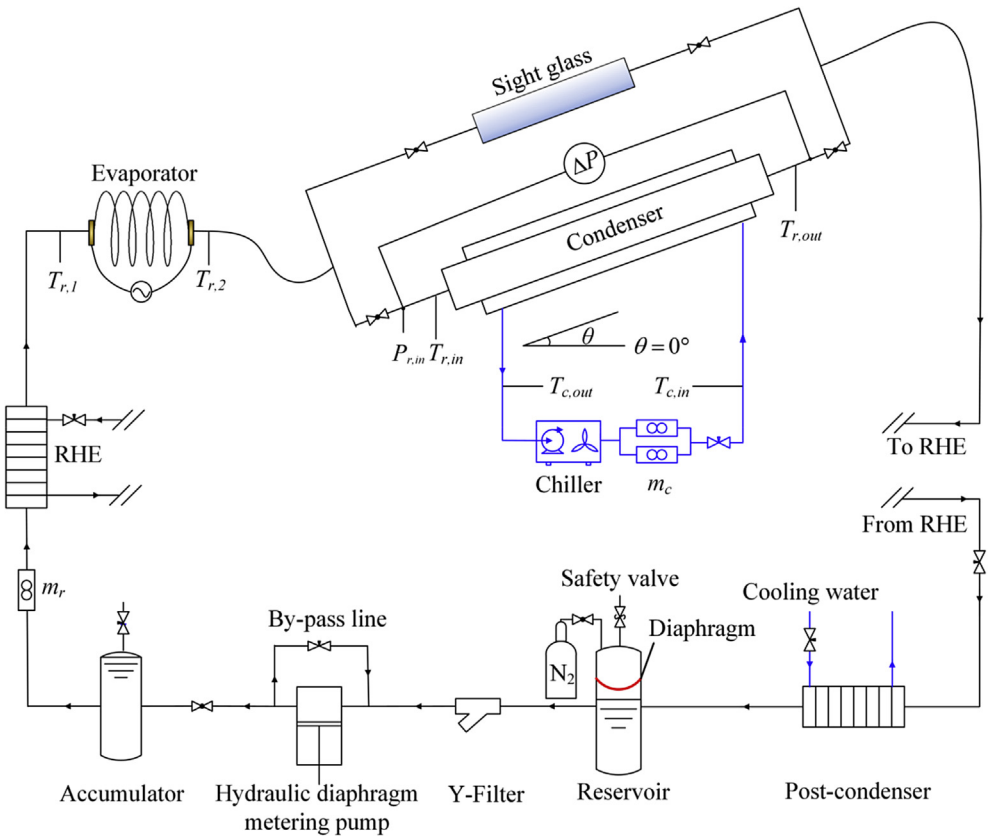

Fig. 1. The experimental setup.

helical coiled tube evaporator, a shell-tube-condenser test section, a chiller water cooling system, and a post-condenser. R245fa liquid in the reservoir was circulated by a hydraulic diaphragm pump, ensuring no lubrication oil in R245fa. Initially, non-condensable gas was removed from the loop and then R245fa liquid was charged into the loop. Pumping flow rate was specified by setting pump frequency and diaphragm displacement. A by-pass line makes it easy to adjust pumping flow rate. An accumulator at the pump outlet stabilized fluid pressure. Liquid levels in the reservoir and accumulator were maintained by adjustable nitrogen gas pressure, noting that nitrogen gas and R245fa liquid were separated by a membrane to ensure no-condensable gas in R245fa. The fluid pressure at the main condenser test section was maintained at about 505 kPa, corresponding to its saturation temperature of 63.1°C. Because our experiment needs higher heating power up to 70 kW, a regenerative heat exchanger was installed before the evaporator to recover heat from the condenser outlet. Then the R245fa fluid was further cooled to liquid in a post-condenser by cooling water.

A helical-coiled tube evaporator heated R245fa liquid by an *AC* (alternative current) electrical power. The evaporator tube had a stretched length of 20.0 m and received a maximum heating power of about 54 kW. The high *AC* voltage was converted to low *AC* voltage by a transformer converter. The evaporator was electrically insulated from other components of the loop. Two copper plates, acting as electrodes, were welded on the curved tube. The curved tube was wrapped by thick thermal insulation material. The voltage and current were measured to obtain the power. The evaporator had subcooled liquid at the inlet, with $T_{r,1}$ as the temperature. $T_{r,2}$ was the outlet temperature, being equal to the two-phase saturation temperature at the outlet. A special test rig was fabricated to have the rotating function. The condenser test section was tightly

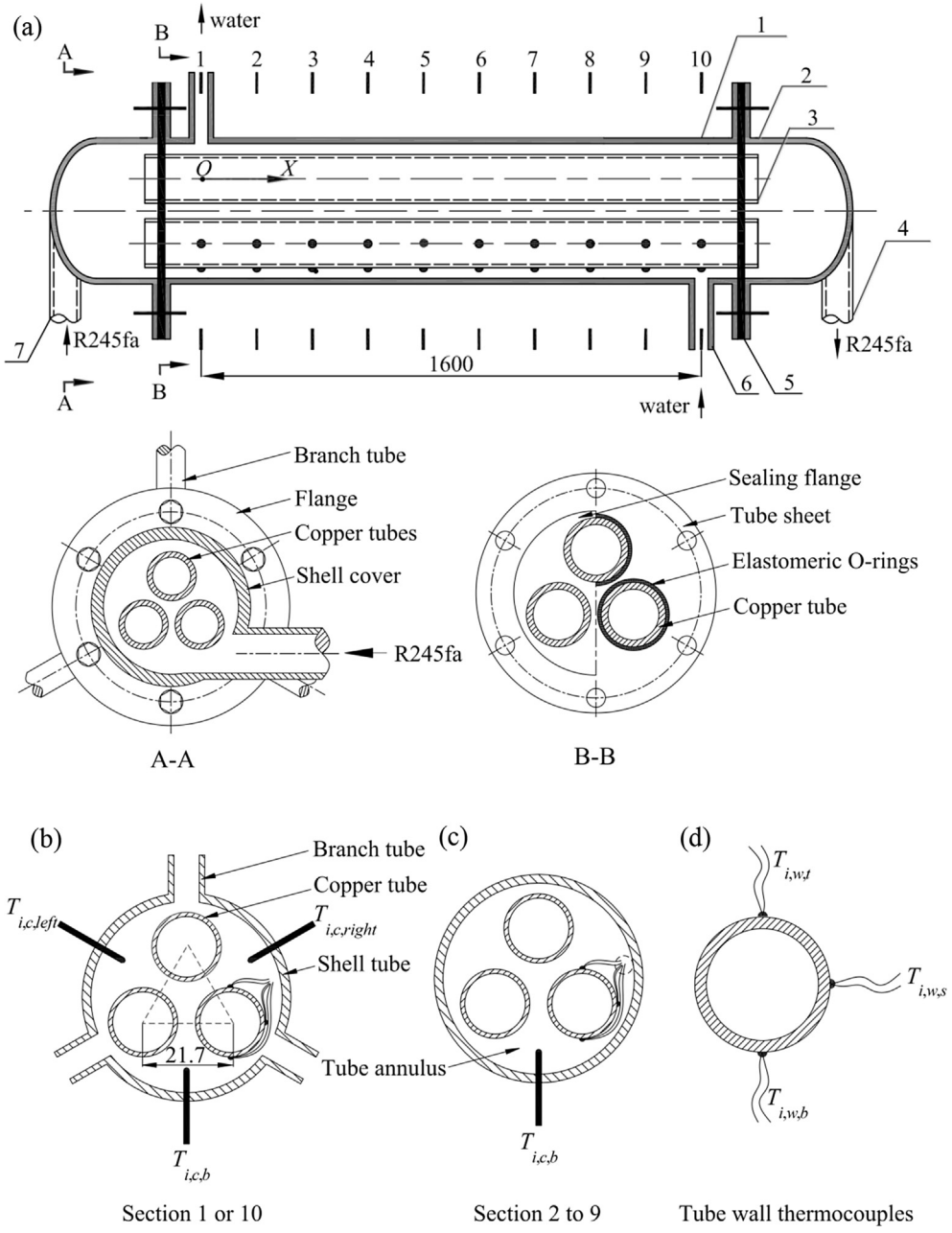

Fig. 2. The condenser test section (1: shell tube, 2:closure head, 3: copper tube, 4: R245fa outlet, 5: tube sheet, 6: cooling water inlet, 7: R245fa inlet).

bonded on the test rig. Inclination angles of condenser flow direction with respect to horizontal position are freely adjusted to have an angle uncertainty of 0.5°. The horizontal flow, inclined up-flow and inclined down-flow refer to $\theta = 0°$, positive θ and negative θ, respectively.

A chiller water loop condensed the two-phase mixture in the test section. The loop included a chiller, a mass flow meter and two jacket thermocouples. The chiller generated a stable chiller water flow rate, m_c, measured by a mass flow meter. The heat was dissipated by a fan to environment. The inlet and outlet temperatures of the chiller water were measured by two thermocouples of $T_{c,in}$ and $T_{c,out}$. The outlet R245fa mixture was further condensed to sub-cooled liquid by the regenerative heat exchanger and post-condenser. The later was cooled by tap water. The tap water was circulated to an outdoor cooling tower, with the maximum cooling capability of about 72 kW.

2.2. Test section

Fig. 2 shows the shell-tube condenser heat exchanger. The pressure vessel had inside and outside diameters of 48.50 mm and 57.08 mm, respectively. It was made of 304 stainless steel. The heat exchanger had a total length of 1850 mm, including two closure heads. The two streams of fluids flow in the condenser in a counter-flow way, with R245fa mixture flowing inside the three tubes and cooling water flowing in shell tube. Each copper tube had an inside diameter of d_i = 14.70 mm and an outside diameter of d_o = 19.02 mm. The effective heat transfer length was $L_e = 1600$ mm. The three tubes were arranged in the shell vessel in a triangle way, with a distance of 21.70 mm between two tubes from center to center.

Fig. 2a shows the R245fa vapor inlet cross section, marked as A-A, and the flange cross section, marked as B-B. In order to ensure uniform distributions of R245fa two-phase mixture in the three tubes, the R245fa mixture entered the closure head tangentially. The flange tightly combined the closure head and the pressure vessel and separated the R245fa fluid and cooling water by a tube sheet, on which there were three holes to penetrate the three copper tubes. Between copper tube and tube sheet was the elastomeric O-ring for sealing purpose. Before the condenser heat exchanger was ready for experiment, leakage was carefully checked to ensure no fluid penetration from one side to another.

Ten cross sections were equally divided along the flow length of 1600 mm. The distance was 177.8 mm between two neighboring cross sections. Cross sections 1 and 10 referred to cooling water outlet and inlet, corresponding to the R245fa fluid inlet and outlet, respectively, (see Fig. 2). In order to see the uniformity of cooling water temperatures at the outlet and inlet cross sections, three thermocouples were symmetrically distributed inside the shell vessel, marked as $T_{i,c,left}$, $T_{i,c,right}$ and $T_{i,c,b}$, in which i refers to the cross section number ($i = 1$ or 10), *c, left, right* and *b* mean cooling water, left corner, right corner and bottom position, respectively. However, on each cross section from 2 to 9, there was only one thermocouple to measure the cooling water temperature, marked as $T_{i,c,b}$ (see Fig. 2c). On each cross section from 1 to 10, three thermocouples were welded on the outside copper tube wall, marked as $T_{i,w,t}$, $T_{i,w,s}$ and $T_{i,w,b}$, in which *i,w, t, s* and *b* referred to cross section number, wall, top, side and bottom position, respectively. All thermocouples were penetrated through miniature holes on the pressure vessel wall and ensured no leakage for such packaging.

In order to explore the complicated condensation heat transfer mechanism, a single glass tube was arranged parallel to the condenser heat exchanger. The R245fa mixture either flowed through the heat exchanger or the glass tube. The R245fa flow can be easily switched between heat transfer and flow visualization measurements by valves. We note that for the flow pattern measurements, high speed images were taken through the glass tube, which was treated as the adiabatic flow pattern cases. The glass tube had identical inside diameter to the copper tube. It can be rotated for the inclination angle variations. For condensation experiment, it is necessary to remove non-condensable gas in the fluid. The present paper used the non-condensable gas removing method reported in Ref. [13]. The good agreement between the measured pressure and saturation temperature at the test section inlet indicated negligible non-condensable gas in R245fa liquid.

This work covered the following data ranges (see Table 1): mass fluxes of R245fa in the range of 198.8–504.7 kg/m^{2}s, vapor mass qualities in the range of 0.291–0.976. Nine inclination angles were tested including 0°, ±5°, ±10°, ±15°, ±30°, in which $\theta = 0°$ represents the horizontal flow, positive and negative angles refer to the inclined up-flow and inclined down-flow, respectively.

2.3. Calibration experiment

The thermal efficiency calibration experiment was performed to obtain the evaporator (helical coiled tube) and condenser efficiencies. The calibration experiment was performed under the single-phase liquid convective heat transfer condition. R245fa has lower specific heat than water. In order to reach similar wall temperature condition as that for R245fa two-phase flow, the calibration experiment used water as the working fluid, instead of R245fa. The evaporator thermal efficiency was

$$\eta_{eva} = \frac{m_w C_{p,w}(T_{w,2} - T_{w,1})}{UI} \tag{1}$$

where m_w and $C_{p,w}$ are the mass flow rate and specific heat of water, respectively. $T_{w,2}$ and $T_{w,1}$ are the water temperatures at the evaporator outlet and inlet, respectively, U and I are the voltage and current, respectively. During the calibration experiment, $T_{w,1}$ was kept about 30°C. The heating power was adjusted so that $T_{w,2}$ was in the range of 60–70 °C, which had similar temperature level as that of the R245fa for the real two-phase experiment. The calibration experiment yielded the measured evaporator thermal efficiency was about 0.91 (average value). The maximum and minimum evaporator efficiencies are 0.916 and 0.903, respectively. For data reduction, the average value was used.

Similar procedure was performed to obtain the condenser efficiency, which was written as

$$\eta_{con} = \frac{m_{w,s} C_{p,(w,s)} \left(T_{(w,s),out} - T_{(w,s),in}\right)}{m_{w,t} C_{p,(w,t)} \left(T_{(w,t),in} - T_{(w,t),out}\right)} \tag{2}$$

where the subscripts (w, t) and (w,s) mean the water in tube side and the water in shell side of shell-tube heat exchanger

Table 1
The experimental running parameters.

Parameters	Range
mass flux, G_r	198.8–504.7 kg/m^{2}s
inlet vapor temperature, $T_{r,in}$	63.1 ± 0.3 °C
inlet vapor pressure, $P_{r,in}$	504.6 ± 5.0 kPa
inlet vapor mass quality, x_{in}	0.291–0.976
heat duties of test section, Q	7.5–15.1 kW
heat flux on the inside wall surface, q	33.78–68.0 kW/m^2
cooling water mass flux, G_c	296.7–302.3 kg/m^{2}s
cooling water inlet temperature, $T_{c,in}$	25.1 ± 0.5 °C
Inclination angle, θ	−30° to 30°

(condenser). The measured average condenser efficiency (η_{con}) reached about 0.98.

The flow resistance and heat transfer calibration experiment directly used R245fa as the working fluid. The measured friction factors of R245fa liquid in turbulent flow regime, reasonably agreed with the Blasius expression [20], with the deviation less than 10.43%. The measured Nusselt numbers matched the Dittus & Boelter correlation well [21], with the relative difference less than 6.37%.

3. Data reduction and uncertainty analysis

3.1. Inlet and outlet vapor mass qualities (x_{in} and x_{out})

The condenser inlet enthalpy ($i_{r,in}$) and quality (x_{in}), come from the evaporator efficiency (η_{eva}, see Section 2.3):

$$i_{r,in} = i_{r,1} + \frac{UI\eta_{eva}}{m_r} \tag{3}$$

$$x_{in} = \frac{i_{r,in} - i_{l,in}}{i_{lg,in}} \tag{4}$$

where $i_{r,1}$ is the R245fa enthalpy at the evaporator inlet, $i_{l,in}$ and $i_{lg,in}$ are the saturated liquid enthalpy and latent heat of evaporation based on the inlet pressure, respectively.

The condenser outlet parameters were computed in terms of the condenser efficiency (η_{con} in Eq. (2)). Heat received by the cooling water in the shell tube is

$$Q = m_c C_{p,c}(T_{c,out} - T_{c,in}) \tag{5}$$

Heat flux based on the inner copper tube wall surface is

$$q = \frac{Q}{3\pi d_i L_e} \tag{6}$$

where L_e is the effective heat transfer length, 3 represents the three copper tubes. The outlet mixture enthalpy and quality are

$$i_{r,out} = i_{r,in} - \frac{Q}{m_r \eta_{con}} \tag{7}$$

$$x_{out} = \frac{i_{r,out} - i_{l,out}}{i_{lg,out}} \tag{8}$$

where $i_{l,out}$ and $i_{lg,out}$ are the saturated liquid enthalpy and latent heat of evaporation based on the outlet pressure, respectively. We note that x_{in} and x_{out} are determined based on the inlet and outlet pressures of R245fa. Both pressures determine latent heat of evaporation of $i_{lg,in}$ and $i_{lg,out}$ in Eqs. (4) and (8). Because the two pressures came from the measured values, yielding accurate predictions of x_{in} and x_{out}. For instance, the inlet pressure measurement involved the uncertainty of 0.2%. When the inlet pressure (P_{in}) varied from 505 kPa to 506 kPa, $i_{lg,in}$ was changed from 165.52 kJ/kg to 165.42 kJ/kg, yielding the relative error of x_{in} of −0.19%.

3.2. Heat transfer coefficients and pressure drops

The R245fa condensation heat transfer coefficient h is based on the average vapor mass quality, written as $x_{ave} = 0.5(x_{in} + x_{out})$. Thus, h is computed as [22]:

$$h = \frac{1}{\frac{1}{h_{to}} - \frac{d_i}{2k_w}\ln\left(\frac{d_o}{d_i}\right) - \frac{d_i}{d_o}\frac{1}{h_c}} \tag{9}$$

where k_w is the thermal conductivity of the copper tube, h_{to} is the total heat transfer coefficient, and h_c is the heat transfer coefficient of cooling water. The determination of h_{to} and h_c can be seen in Ref. [13].

The present paper also involved pressures drop, which was correlated based on the Chisholm method [23], in which the two-phase multiplier ratio ϕ_l is defined as

$$\phi_l = \sqrt{\frac{\Delta P_{TP,f}}{\Delta P_{l,f}}} \tag{10}$$

where $\Delta P_{TP,f}$ and $\Delta P_{l,f}$ are the two-phase friction pressure drop and friction pressure drop if liquid flows alone. The Lockhart-Martinelli parameter X is

$$X = \sqrt{\frac{\Delta P_{l,f}}{\Delta P_{g,f}}} \tag{11}$$

where $\Delta P_{g,f}$ is the friction pressure drop if vapor phase flows alone. Finally, the following equation is written to correlate the two-phase friction pressure drop.

$$\phi_l^2 = 1 + \frac{C}{X} + \frac{1}{X^2} \tag{12}$$

The C values are correlated based on our experimental data using Eq. (12).

OMEGA K-type thermocouples were carefully calibrated, having 0.1°C uncertainty. Two DMF-1-DX mass flow meters, one for R245fa and the other for cooling water, measured mass flow rates of the two fluids, having the accuracy of 0.1%. Both *AC* voltage and current had the uncertainties of 0.1%. IPC was used as the data acquisition system, having 100 channels for signal processing. Uncertainties of vapor mass qualities and heat transfer coefficient were evaluated in terms of the error transmission theory [24]. Heat transfer coefficient (h), vapor mass qualities (x) and heat fluxes (q) had the accuracies of 5.47%, 5.86% and 5.43%, respectively.

4. Results and discussion

4.1. Comparison of our experimental data with available correlations

This section compared our experimental data with available correlations in the literature. We define the deviation parameters first

$$e = \frac{h_{pre} - h_{exp}}{h_{exp}} \times 100\% \tag{13}$$

$$e_R = \frac{1}{n}\sum_1^n \left[\frac{h_{pre} - h_{exp}}{h_{exp}}\right] \times 100\% \tag{14}$$

$$e_A = \frac{1}{n}\sum_1^n \left[\frac{|h_{pre} - h_{exp}|}{h_{exp}}\right] \times 100\% \tag{15}$$

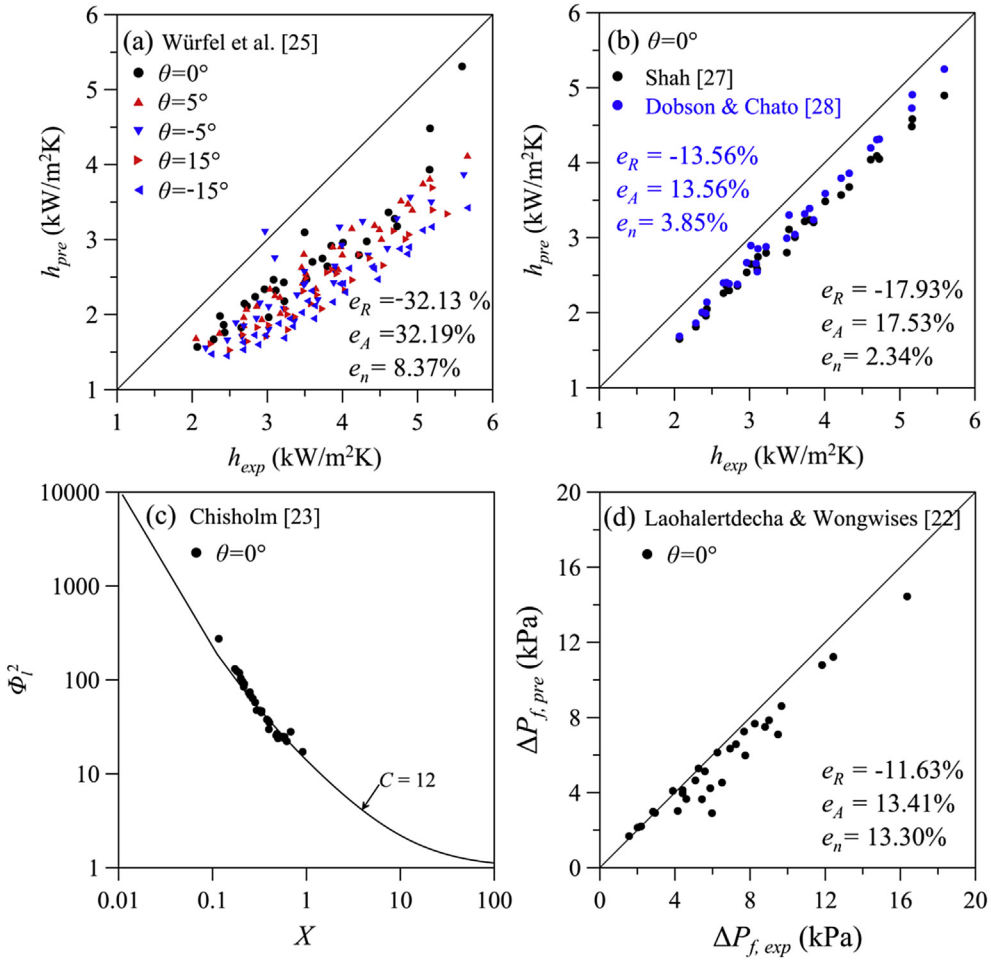

Fig. 3. Comparison between measured and predicted heat transfer coefficients and pressure drops.

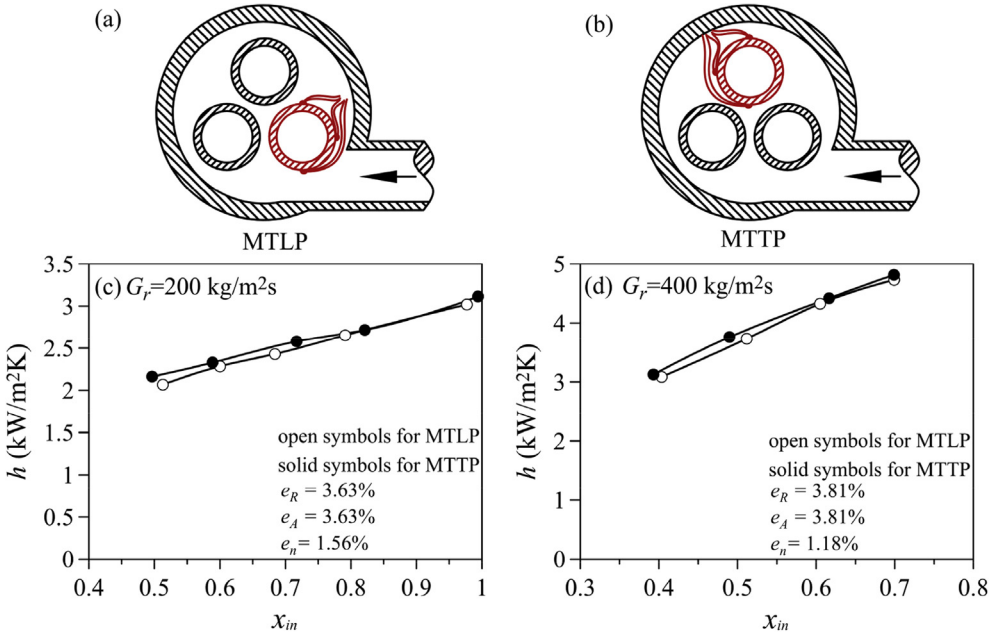

Fig. 4. Comparison of condensation heat transfer coefficients for MTLP (measured tube at the lower position) and MTTP (measured tube at the top position), a: MTLP arrangement, b: MTTP arrangement, c: comparison at G_r = 200 kg/m^{2}s, d: comparison at G_r = 400 kg/m^{2}s, θ = 0°.

$$e_n = \left\{ \left[\sum_1^n (e - e_R)^2 \right] \Big/ (n-1) \right\}^{1/2} \times 100\% \quad (16)$$

where e is called deviation, e_R, e_A, e_n are called average deviation, mean absolute deviation and standard deviation, respectively, n was the number of data samples. The smaller the deviations, the correlations are more accurate to match our experimental data.

Fig. 3a shows the comparison between our condensation heat transfer coefficients and the correlation by Würfel et al. [25]. Data with five inclination angles including $\theta = 0°$, $-5°$, $5°$, $-15°$ and $15°$ are presented. The three deviation values e_R, e_A and e_n reached 32.13%, 32.19% and 8.37%, respectively, showing larger deviations. Ref. [26] noted that the effect of gravity force on condensation heat transfer is not well understood and needs further investigation.

Fig. 3b shows better match of our condensation heat transfer coefficients at horizontal position ($\theta = 0°$) with the predictions by both Shah [27] and Dobson & Chato [28]. The deviation e_R is −17.93%, which is acceptable for phase change heat transfer.

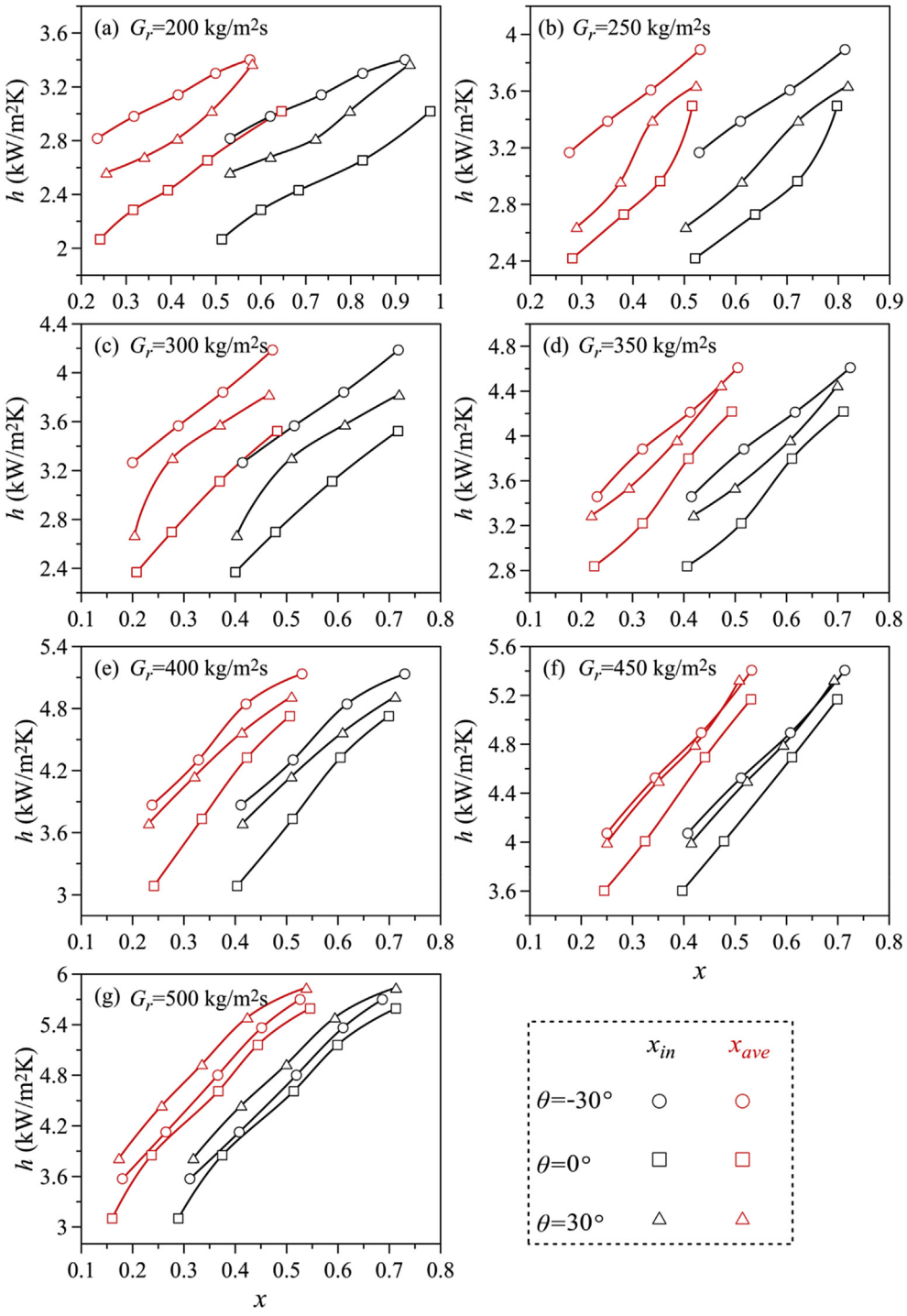

Fig. 5. Condensation heat transfer coefficients versus vapor mass qualities.

For horizontal position, ϕ_l^2 based on our two-phase frictional pressure drop is well correlated by the Chisholm method with $C = 12$ (see Fig. 3c). Fig. 3d shows that our measured two-phase friction pressure drops are well matched the correlation of Laohalertdecha & Wongwises [22]. $C = 12$ is also suitable for the friction pressure drop prediction at inclined positions ($\theta = -30°$-$30°$). The total pressure drop ΔP includes three components of ΔP_f (friction pressure drop), ΔP_a (acceleration pressure drop) and ΔP_g (gravity pressure drop): $\Delta P = \Delta P_f + \Delta P_a + \Delta P_g$. When ΔP_a and ΔP_g are computed using the homogeneous model of two-phase flow [29], and ΔP_f is predicted by Eq. (12) with $C = 12$, the maximum difference between predicted total pressure drops and measured ones is 15%, which is acceptable for two-phase flow. Therefore, the present paper focused on the investigation of the condensation heat transfer.

We note that most of available studies used the single tube as the test section to investigate condensation heat transfer of refrigerant [16–18]. The results are difficult to be directly extended in a condenser (or call heat exchanger) with multi-tubes. This is because flow rates of refrigerant in different tubes may be different, depending on the inlet fluid plenum. This paper directly used the shell-tube condenser having three tubes as the test section. In order to ensure quasi-uniform flow rate distribution in different tubes, significant improvement was performed for the inlet fluid plenum design (see Fig. 2a), in which vapor tangentially entered the inlet fluid plenum. This design is expected to improve the flow rate distribution. An indirect method verified the effectiveness of the inlet fluid plenum design. During the calibration experiment, condensation heat transfer coefficients were obtained when the measured tube was at the top location (MTTP) and at the lower position (MTLP in Fig. 4). Condensation heat transfer coefficients for MTTP deviate less from those for MTLP, at $G_r = 200$ or 400 kg/m^{2}s (see Fig. 4). The maximum difference of h is 4.87%. This calibration indicated quasi-uniform flow rate distribution in the three tubes, showing small effect of gravity on the flow rate distribution by using the tangential entering method. Thus, results in this paper are suitable for the condensation design of both single-tube and multi-tubes.

4.2. Condensation heat transfer coefficients

Fig. 5 shows condensation heat transfer coefficients, h, versus x_{in} or x_{ave}. Condensation heat transfer coefficients are quasi-linearly increased with both x_{in} and x_{ave}. Different h ranges are used in different subfigures to show increased condensation heat transfer coefficients by raising R245fa mass fluxes G_r. The increased h with both vapor mass qualities x and mass fluxes G_r indicates the inertia force effect on condensation heat transfer. Fig. 5 shows the horizontal position ($\theta = 0°$) possessing lowest condensation heat transfer coefficients among the three inclination angles of $\theta = -30°$, $0°$ and $30°$. The difference of heat transfer coefficients among the three inclination angles is larger at lower mass flux of $G_r = 200$ kg/m^{2}s, but becomes smaller when G_r is increased. Gravity force plays an important role to influence heat transfer at low mass flux, but the gravity effect is weakened at larger mass flux, showing competitive balance between inertia force and gravity force. Fig. 6 demonstrates the quasi-linear relationship of h against G_r.

Much attention is paid to h dependent on θ in Fig. 7. Three inlet vapor mass qualities of $x_{in} = 0.4$, 0.6 and 0.8 are shown. We plot $h/h_{\theta=0°}$ versus θ, representing condensation heat transfer coefficient at any inclination angle θ related to that at the horizontal position. It is found $h/h_{\theta=0°}>1$ if the inclination angle deviates from the horizontal position. Both weakly inclined up-flow and down-flow enhance condensation heat transfer, with $\theta = -30°$ to $30°$. Section 4.3 will give the mechanism.

4.3. Flow pattern observations

Five flow patterns were observed: stratified-wavy (*SW*), stratified-smooth (*SS*), intermittent flow (*I*), churn flow (*C*) and annular flow (*A*). The flow pattern definition can be found in Taitel & Dukler [30] and Taitel et al. [31]. The stratified-smooth (*SS*) flow happens when the liquid layer height signal is stable. If the liquid layer thickness signal becomes oscillating, the stratified-wavy (*SW*) flow is called. When the wave crest of the stratified-wavy flow reaches the top of tube wall, the intermittent flow (*I*) occurs. The *SW* and *I* flows involve apparent interface waves, which are explained later. The smaller surface tension force and larger tube diameter destroy the occurring criterion of bubble flow and slug flow, thus, the two flow patterns are not observed here.

Fig. 8 demonstrates flow pattern maps at $\theta = 0°$, $-15°$, $15°$, $-30°$

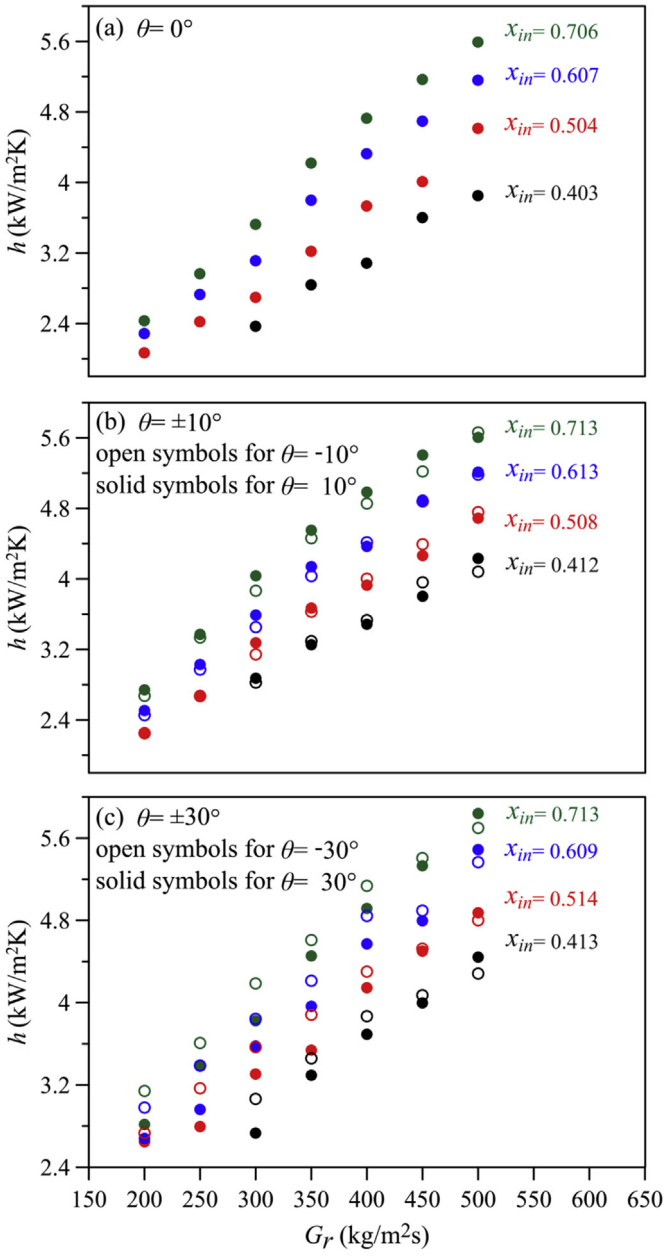

Fig. 6. Condensation heat transfer coefficients versus mass fluxes.

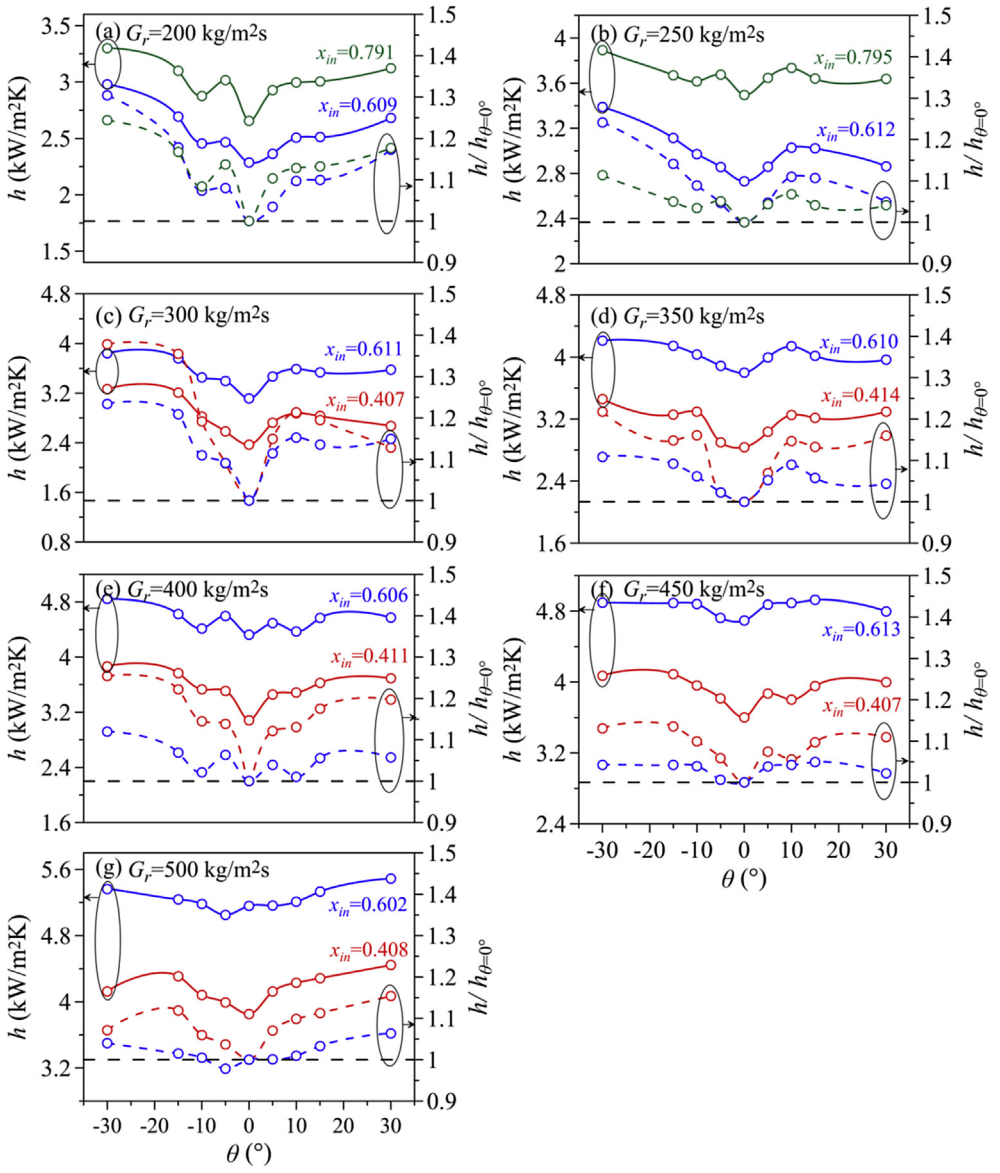

Fig. 7. Effect of inclination angles on condensation heat transfer coefficients.

and 30°. Fig. 8a shows flow pattern map for horizontal position, in which annular flow (*A*), intermittent flow (*I*) and stratified-wavy flow (*SW*) are included. The determined transition boundaries are roughly matched those predicted by Hajal et al. [32]. Fig. 8b–c identified the effect of inclined up-flow and down-flow on flow patterns. At $\theta = -15°$, three flow patterns appear as annular flow (*A*), stratified-wavy flow (*SW*) and stratified-smooth flow (*SS*) (Fig. 8b). Instead, the inclined up-flow possess intermittent flow (*I*) and stratified-wavy flow (*SW*) (Fig. 8c). The inclined up-flow behaves more unstable. Fig. 8d–e yields similar conclusion. The inclined down-flow of $\theta = -30°$ has the *A* and *SS* flow patterns, except a small *SW* regime, but for inclined up-flow, *SW* and *C* flow patterns appear, showing "turbulent" characteristic (see Fig. 8e).

The unstable behavior at the inclined up-flow is related to the vapor-liquid interface wave. The dynamic liquid films at the tube bottom were acquired with high speed images by analyzing the gray gradient of videos. The non-dimensional liquid height (h_l/d_i) and standard deviation of the dimensionless liquid height (σ_l) are defined as

$$(h_l/d_i)_{ave} = \frac{1}{n}\sum_{1}^{n}(h_l/d_i) \tag{17}$$

$$\sigma_l = \left\{\frac{\sum_1^n [h_l/d_i - (h_l/d_i)_{ave}]^2}{n-1}\right\}^{1/2} \tag{18}$$

where the subscript *ave* means the average value and *n* referred to the number of data samples. The bottom wall and top wall corresponded to $h_l/d_i = 0$ and 1, respectively, d_i was the inner tube diameter. The larger standard deviation of h_l/d_i shows more unstable vapor-liquid interface.

Fig. 9 shows h_l/d_i versus time at $\theta = -15°$, 0° and 15°. The average h_l/d_i values are increased from 0.381 to 0.476, showing the increased liquid heights when the inclination angles are increased from $\theta = -15°$ to 15°. On the other hand, the standard deviation of

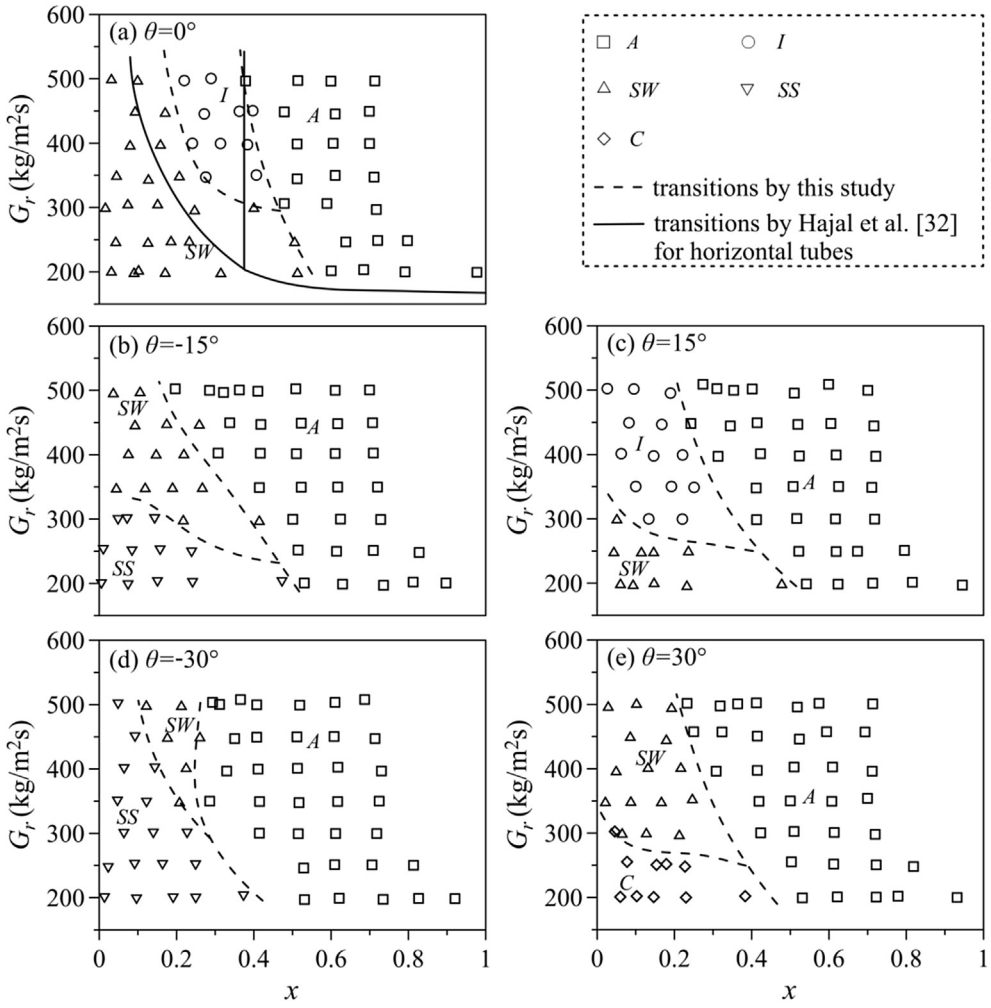

Fig. 8. Flow pattern maps at five inclination angles (*A*: annular flow, *I*: intermittent flow, *SW*: stratified-wavy flow, *SS*: stratified-smooth flow, *C*: churn flow).

the dimensionless liquid height (σ_l) gets small value of 0.017 at $\theta = -15°$, behaving very stable, but σ_l reached larger value of 0.109 at $\theta = 15°$, behaving unstable interface for inclined up-flow.

4.4. Connection of condensation heat transfer with flow pattern observations

This section gave the connection between condensation heat transfer coefficients and flow patterns. Non-dimensional parameters involved in two-phase systems are [28].

$$Fr = \frac{G^2}{\rho_l^2 g d_i} \tag{19}$$

$$Fr_l = \frac{G^2(1-x_{ave})^2}{\rho_l^2 g d_i} \tag{20}$$

$$Fr_g = \frac{G^2 x_{ave}^2}{\rho_g^2 g d_i} \tag{21}$$

$$X = \left(\frac{1-x_{ave}}{x_{ave}}\right)^{0.9}\left(\frac{\rho_g}{\rho_l}\right)^{0.5}\left(\frac{\mu_l}{\mu_g}\right)^{0.1} \tag{22}$$

$$Bd = \frac{g\left(\rho_l - \rho_g\right)d_i}{\sigma} \tag{23}$$

$$We = \frac{G^2 d_i}{\rho_l \sigma} \tag{24}$$

where *Fr*, Fr_l, Fr_g, *X*, *Bd* and *We* are the Froude number, Froude number of liquid phase, Froude number of vapor phase, Martinelli number, Bond number and Weber number, ρ, μ and σ are density, viscosity and surface tension, respectively, g is the gravity acceleration.

Here, Froude number was in the range of $Fr = 0.178-1.185$, indicating important roles of both inertia force and gravity force. Bond number was $Bd = 17554$, indicating negligible surface tension effect compared with gravity. Weber number was in the range of $We = 47-571$, indicating less importance of surface tension compared with inertia force. This analysis shows the system governed by inertia force and gravity force to yield the Froude number dominant mechanism.

Flow patterns have strong connection with condensation heat

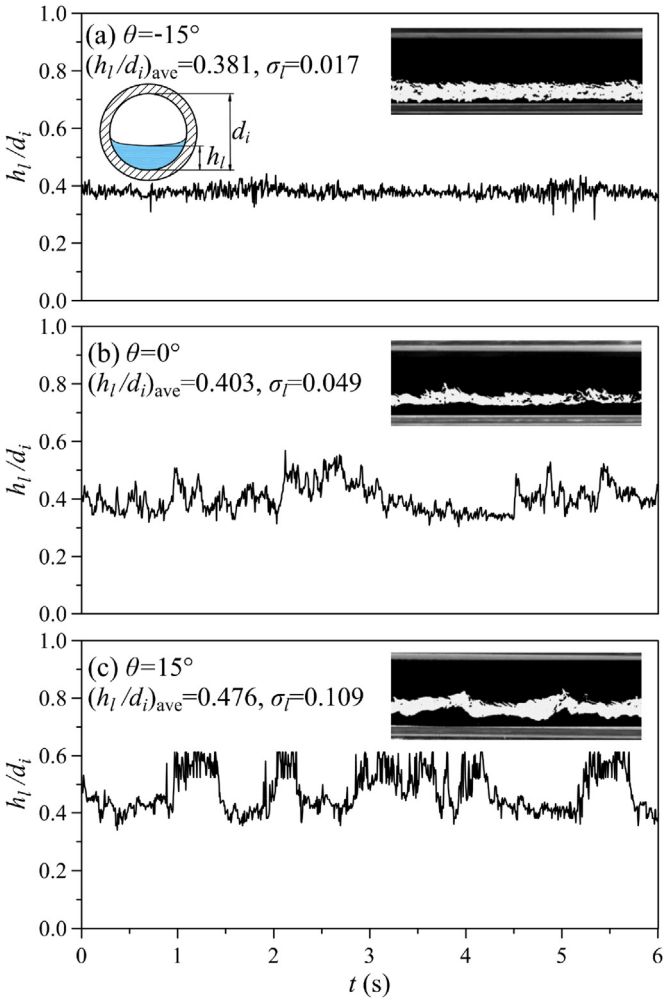

Fig. 9. The liquid height signal versus time at G_r = 201.6 kg/m^{2}s and x = 0.247.

transfer. For inclined up-flow, a negative gravity force component acts on the flow direction, resisting the inertia force induced motion and increasing the shear stress on vapor-liquid interface. This triggers vapor-liquid interface wave to behave unstable nature. Two mechanisms are competed to determine condensation heat transfer coefficients. First, the increased liquid layer thickness on the tube bottom deteriorates condensation heat transfer. Second, the unstable vapor-liquid interface enhances condensation heat transfer due to the strong mass and momentum exchange across the vapor-liquid interface. The comprehensive effect yields enhanced condensation heat transfer with inclined up-flow than with horizontal flow. For inclined down-flow, the gravity force component along the flow direction is co-current to the inertia force, accelerating the liquid layer motion. The decreased liquid layer thickness on the tube bottom accounts for the condensation heat transfer enhancement for inclined down-flow compared with horizontal flow. The analysis yields smallest condensation heat transfer coefficient at horizontal position with θ from −30° to 30°. Both inclined up-flow and down-flow increase condensation heat transfer coefficients.

4.5. Correlation of condensation heat transfer coefficients with respect to θ

This section gave our h correlation versus θ. Because θ has a narrow range from −30° to 30°, h is correlated as a linear relationship with θ.

$$\frac{h}{h_{\theta=0^\circ}} = 1 + a\theta \tag{25}$$

Because minimum h is reached at $\theta = 0^\circ$, our correlation yields two regimes for $\theta > 0$ and $\theta < 0$, respectively. We recall the Froude number Fr ~1, but the Froude number of vapor phase, Fr_g, represents inertia force related to vapor density, having a range of 18.2–688.1. For inclined up-flow, Fr_g influences liquid layer thickness on the tube bottom and vapor-liquid interface wave, to determine condensation heat transfer. For inclined down-flow, Fr_g influences liquid layer thickness on the tube bottom to affect condensation heat transfer.

We plot a versus Fr_g in Fig. 10a for $\theta > 0$ and Fig. 10b for $\theta < 0$. values of a are decreased with increases of Fr_g, consistent with our understanding that the inclination angle effect disappears at large Fr_g. We also show that the a values are larger for smaller inclination angles. For example, the data points at $\theta = 5^\circ$ are above those at other inclination angles. Using the arc unit of θ and for $0<\theta\leq\frac{\pi}{6}$, a is

$$a = a_{\theta=\pi/36} + \frac{\theta - \pi/36}{\pi/6 - \pi/36}\left(a_{\theta=\pi/6} - a_{\theta=\pi/36}\right) \tag{26}$$

where $a_{\theta=\pi/36} = \frac{4.9845}{Fr_g^{0.3794}}$ and $a_{\theta=\pi/6} = \frac{2.4602}{Fr_g^{0.5162}}$.

For $-\frac{\pi}{6} \leq \theta < 0$, a is

$$a = a_{\theta=\pi/36} + \frac{\theta - \pi/36}{\pi/6 - \pi/36}\left(a_{\theta=-\pi/36} - a_{\theta=-\pi/6}\right) \tag{27}$$

where $a_{\theta=-\pi/36} = \frac{5.0826}{Fr_g^{0.4067}}$ and $a_{\theta=-\pi/6} = \frac{4.4522}{Fr_g^{0.5534}}$.

Equation (26) determined a based on the linear interpolation with respect to θ in terms of the curve fits at $a_{\theta=\pi/36}$ and $a_{\theta=\pi/6}$, for inclined up-flow. Alternatively, a was determined in terms of the curve fits at $a_{\theta=-\pi/36}$ and $a_{\theta=-\pi/6}$, for inclined down-flow (see Eq. (27)). Because a in Eq. (25) has a linear relationship with θ, condensation heat transfer coefficients h has a parabolic curve versus θ. We gave our measured h compared with predictions in Eqs.(25)–(27). The correlation well reflects the change trends of h with respect to θ. Fig. 10c–f shows the comparisons for four cases with different G_r and x_{in}. Containing 240 data points, the deviation parameters of e_R, e_A and e_n are less than 5%.

Our heat transfer correlation covers the mass fluxes of G_r = 200–500 kg/m^{2}s, vapor mass qualities of x = 0.29–0.98, and inclination angles θ from −30° to 30°. R245fa was the working fluid. The test tube had an inside diameter of 14.70 mm and a length of 1600 mm. The correlation is suitable for both single-tube and multi-tubes, if the flow distributions are uniform between different tubes. For horizontal position, our measured condensation heat transfer coefficients matched the correlation of Shah [27] and Dobson & Chato [28] (see Fig. 3). Our work focused on the analysis of inclination angle effect. The θ effect is considered by the non-dimensional parameter analysis, covering the ranges of Fr = 0.178–1.185 (Froude number) and We = 47–571 (Weber number). The correlation can be extended to other condensation conditions if Fr and We cover the given ranges. Such extension should be verified by future investigations.

The present work limits the inclination angle (θ) ranges from −30° to 30°. This is because most of condenser heat exchangers are arranged at the horizontal position or weakly inclined position. Besides, previous studies [33,34] indicated that the condensation heat transfer coefficients are more complicated for the weakly inclined situation. It is expected that condensation heat

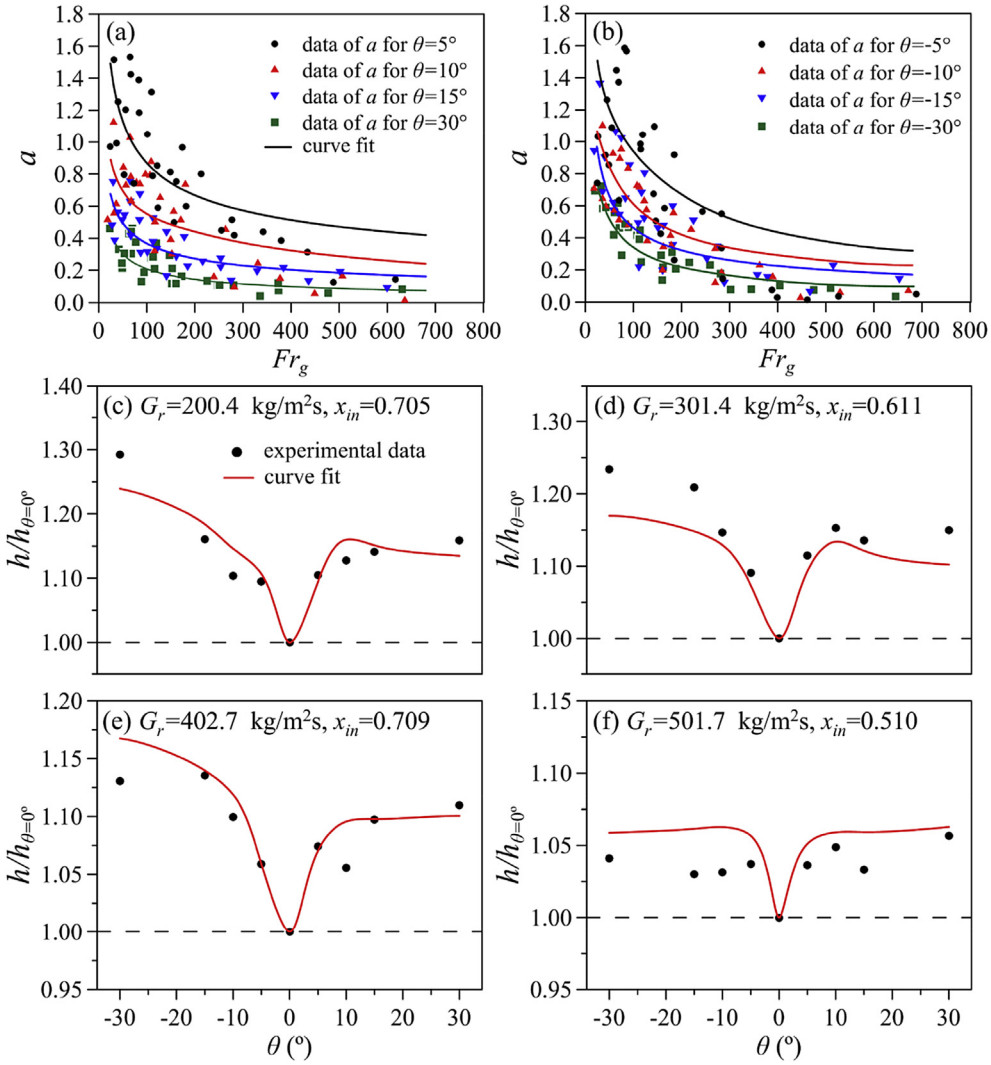

Fig. 10. Comparison of condensation heat transfer coefficients between predictions and measured ones, a and b: a versus Fr_g, c–f: $h/h_{\theta=0°}$ versus θ.

transfer coefficients may be further increased for the inclination angles less than −30°, due to the further decreased liquid film thickness on the tube wall. However, the increase trend should be restricted with continuous variation of inclination angles. This is because heat transfer is not only governed by liquid film thickness, but also controlled by flow patterns. The stratified flow may be switched to other flow patterns such as slug flow if θ is changed too much.

5. Conclusions

Condensation heat transfer of R245fa was investigated in a shell-tube condenser heat exchanger. Heat transfer coefficients were measured covering wide range of parameters. Much attention was paid to the effect of inclination angles on the thermal performance. Flow pattern and dynamic liquid height were measured to explore the embedded mechanisms.

Condensation heat transfer coefficients are increased with increases of mass fluxes and vapor mass qualities. They yield minimum values at the horizontal position with the inclination angles from −30° to 30°. Both inclined up-flow and down-flow enhance condensation heat transfer. Flow patterns are measured to include stratified-smooth flow (*SS*), stratified-wavy flow (*SW*), intermittent flow (*I*), churn flow (*C*) and annular flow (*A*). Inclination angles apparently influence flow patterns. The flow is stable for inclined down-flow but becomes more unstable for inclined up-flow. The liquid height signal identified the vapor-liquid interface wave as the mechanism to be unstable for inclined up-flow.

The non-dimensional parameters involved in two-phase system identified the competition between inertia force and gravity force. Due to the larger tube diameter and smaller surface tension, the surface tension force is less important for condensation heat transfer of R245fa. Condensation heat transfer coefficients were correlated based on the Froude number of vapor phase and inclination angles. The correlation well matched the experimental data.

Acknowledgements

The authors thank for the funding support from Natural Science Foundation of China with contract numbers of 51436004 and 51210011, and the Fundamental Research Funds for the Central Universities (2016XS23).

References

[1] Freni A, Maggio G, Sapienza A, Frazzica A, Restuccia G, Vasta S. Comparative analysis of promising adsorbent/adsorbate pairs for adsorptive heat pumping,

air conditioning and refrigeration. Appl Therm Eng 2016;104:85–95.
[2] Ramesh PS, Biplab C, Ranadip KD. A review on low grade heat powered adsorption cooling systems for ice production. Renew Sust Energ. Rev 2016;62:109–20.
[3] Cabello R, Sánchez D, Llopis R, Arauzo I, Torrella E. Experimental comparison between R152a and R134a working in a refrigeration facility equipped with a hermetic compressor. Int J Refrig 2015;60:92–105.
[4] Wang X, Yu JL. An experimental investigation on a novel ejector enhanced refrigeration cycle applied in the domestic refrigerator-freezer. Energy 2015;93:202–9.
[5] Wang CC, Chiang CS, Yu JG. An experimental study of in-tube evaporation of R-22 inside a 6.5-mm smooth tube. Int J Heat Fluid Fl 1998;19:259–69.
[6] Mendoza-Miranda JM, Mota-Babiloni A, Navarro-Esbrí J. Evaluation of R448A and R450A as low-GWP alternatives for R404A and R134a using a micro-fin tube evaporator model. Appl Therm Eng 2016;98:330–9.
[7] Xu J, Yu C. Critical temperature criterion for selection of working fluids for subcritical pressure Organic Rankine cycles. Energy 2014;74:719–33.
[8] Shu GQ, Liu LN, Tian H, Wei HQ, Yu GP. Parametric and working fluid analysis of a dual-loop organic Rankine cycle (DORC) used in engine waste heat recovery. Appl Therm Eng 2014;113:1188–98.
[9] Yang Z, Wu X, Peng JJ. Theoretical and experimental investigation on the flame-retarding characteristic of R245fa. Exp Therm Fluid Sci 2013;44:613–9.
[10] Zhelezny VP, Semenyuk YV, Ancherbak SN, Grebenkov AJ, Beliayeva OV. An experimental investigation and modelling of the solubility, density and surface tension of 1,1,1,3,3-pentafluoropropane(R-245fa)/synthetic polyolester compressor oil solutions. J Fluor Chem 2007;128:1029–38.
[11] Yang MH, Yeh RH. Thermodynamic and economic performances optimization of an organic Rankine cycle system utilizing exhaust gas of a large marine diesel engine. Appl Energy 2015;149:1–12.
[12] Wang X, Liu XM, Zhang CH. Parametric optimization and range analysis of Organic Rankine Cycle for binary-cycle geothermal plant. Energy Convers. Manage 2014;80:256–65.
[13] Xie J, Xu J, Cheng Y, Xing F, He X. Condensation heat transfer of R245fa in tubes with and without lyophilic porous-membrane-tube insert. Int J Heat Mass Tran 2015;88:261–75.
[14] Cavallini A, Bortolin S, Col DD, Matkovic M, Paria S, Rossetto L. Condensation heat transfer and pressure losses of high and low pressure refrigerants flowing in a single circular minichannel. Heat Transf Eng 2011;32:90–8.
[15] Al-Hajri EA, Shooshtari AH, Dessiatoun S, Ohadi MM. Performance characterization of R134a and R245fa in a high aspect ratio microchannel condenser. Int J Refrig 2013;36:588–600.
[16] Ghim G, Lee J. Experimental evaluation of the in-tube condensation heat transfer of pure n-pentane/R245fa and their non-azeotropic mixture as an ORC working fluid. Appl Therm Eng 2016;106:753–61.
[17] Lips S, Meyer JP. Experimental study of convective condensation in an inclined smooth tube. Part I: inclination effect on flow pattern and heat transfer coefficient. Int J Heat Mass Tran 2012;55:395–404.
[18] Mohseni SG, Akhavan-Behabadi MA, Saeedinia M. Flow pattern visualization and heat transfer characteristics of R-134a during condensation inside a smooth tube with different tube inclinations. Int J Heat Mass Tran 2013;60:598–602.
[19] Gupta R, Fletcher DF, Haynes BS. Taylor flow in microchannels: a review of experimental and computational work. Int J Com Multiphas Flow 2010;2:1–32.
[20] Tropea C, Yarin AL, Foss JF. Springer handbook of experimental fluid mechanics, vol. 1. Springer; 2007.
[21] Dittus FW, Boelter LMK. Heat transfer in automobile radiators of the tubular type. Int Commun Heat Mass Tran 1985;12:3–22.
[22] Laohalertdecha S, Wongwises S. The effects of corrugation pitch on the condensation heat transfer coefficient and pressure drop of R-134a inside horizontal corrugated tube. Int J Heat Mass Tran 2010;53:2924–31.
[23] Chisholm D. A theoretical basis for the Lockhart-Martinelli correlation for two-phase flow. Int J Heat Mass Tran 1967;10:1767–78.
[24] Holman JP, Gajda WJ. Experimental methods for engineers. fourth ed. New York: McGraw-Hill; 1994.
[25] Würfel R, Kreutzer T, Fratzscher W. Turbulence transfer processes in adiabatic and condensing film flow in an inclined tube. Chem Eng Technol 2003;26:439–48.
[26] Lips S, Meyer JP. Two-phase flow in inclined tubes with specific reference to condensation: a review. Int J Multiphas Flow 2011;37:845–59.
[27] Shah MM. An improved and extended general correlation for heat transfer during condensation in plain tubes. HVAC&R RES 2009;15:889–91.
[28] Dobson MK, Chato JC. Condensation in smooth horizontal tubes. J Heat Trans 1998;120:193–213.
[29] Collier JG, Thome JR. Convective boiling and condensation. 3th ed. New York: Oxford University Press; 1994.
[30] Taitel Y, Dukler AE. A model for predicting flow regime transitions in horizontal and near horizontal gas-liquid flow. AICHE J 1976;22:47–55.
[31] Taitel Y, Bornea D, Dukler AE. Modelling flow pattern transitions for steady upward gas-liquid flow in vertical tubes. AICHE J 1980;26:345–54.
[32] Hajal JE, Thome JR, Cavallini A. Condensation in horizontal tubes, part 1: two-phase flow pattern map. Int J Heat Mass Tran 2003;46:3349–63.
[33] Meyer JP, Dirker J, Adelaja AO. Condensation heat transfer in smooth inclined tubes for R134a at different saturation temperatures. Int J Heat Mass Tran 2014;70:515–25.
[34] Adelaja AO, Dirker J, Meyer JP. Convective condensation heat transfer of R134a in tubes at different inclination angles. Int J GREEN ENERGY 2016;13:812–21.

Nomenclature

A: annular flow
a: coefficient in Eq. (25)
AC: alternative current
Bd: Bond number
C: churn flow
C_p: specific heat at constant pressure J/kg K
d: diameter m
e: deviation
e_R: average deviation
e_A: average absolute deviation
e_n: standard deviation
Fr: Froude number
G: mass flux kg/m^{2}s
g: acceleration of gravity m/s^2
h: heat transfer coefficient W/m^{2}K
h_l: liquid height m
i: enthalpy J/kg
I: current A
I: intermittent flow
k: thermal conductivity W/(mK)
L: length m
m: mass flow rate kg/s
n: number of data points
P: pressure Pa
ΔP: pressure drop Pa
q: heat flux on the inner wall surface W/m^2
Q: heat transfer rate W
SS: stratified-smooth flow
SW: stratified-wavy flow
t: time s
T: temperature ^{o}C or K
MTLP: measured tube at the lower position
MTTP: measured tube at the top position
U: voltage V
We: Weber number
X: Martinelli parameter
x: vapor mass quality

Greek symbols

θ: inclination angle
η: thermal efficiency
ρ: density kg/m^3
μ: viscosity Pa·s
σ: surface tension N/m
σ_l: standard deviation of the dimensionless liquid height
ϕ_l^2: two-phase flow multiplier

Subscript

1: evaporator inlet
2: evaporator outlet
a: acceleration pressure
ave: average
b: bottom wall location
c: cooling water
con: condenser
e: effective heat transfer
eva: evaporator
exp: experiment
f: frictional pressure
g: vapor or gravity pressure
i: inside wall surface
in: condenser inlet
l: liquid
left: left corner
o: outer wall surface
out: condenser outlet
pre: prediction
r: organic fluid (R245fa in this study)
right: right corner
s: side wall location or shell side
t: top wall location or tube side
to: total
TP: two-phase flow
w: wall or water